# Nonlinear optical generation of entangled squeezed states in lossy nonorthogonal quasimodes: an analytic solution

Colin Vendromin\* and Marc M. Dignam
Department of Physics, Engineering Physics, and Astronomy,
Queen's University, Kingston, Ontario, Canada, K7L 3N6
(Dated: October 14, 2022)

We prove that the density operator for the nonlinearly-generated quantum state of light in the M lossy nonorthogonal quasimodes of a nanocavity system has the analytic form of a multimode squeezed thermal state, where the time-dependence of the squeezing and thermal photon parameters are given by a set of 3M coupled differential equations. We apply our approach to a system with two highly nonorthogonal quasimodes and obtain good agreement with simulations using a basis of Fock states. Our approach provides an efficient way to model and optimize the generation of mixed Gaussian cluster states.

Squeezed states of light are the fundamental states used to generate multimode entangled states for continuous variable quantum computing [1]. Multimode entangled states can be made by propagating a series of squeezed states through an array of linear optical elements, which collectively act to entangle the modes in both frequency and time [2–5]. Alternatively, they can be generated directly in multimode nanocavity systems using the nonlinear optical processes of spontaneous fourwave mixing (SFWM) or parametric down conversion (PDC) [6]. Using the first approach, it has been demonstrated experimentally that three-dimensional cluster states can be generated, which can be used to make a universal quantum computer [7]. Using the second approach, universal continuous-variable cluster states have been created using an optical parametric oscillator (OPO), where the quantum information is encoded in the quadratures of the optical frequency comb of the OPO [8, 9]. Also, cluster states have been generated using a ring resonator [10], where the squeezed modes are simultaneously entangled in frequency and time. In this paper, we use the second approach and theoretically study the generation of multimode entangled states via SFWM in a general lossy multimode structure.

Theoretical studies on continuous-variable cluster states have largely focused on the generation of a multimode squeezed vacuum state (MSVS), a pure Gaussian state, where the scattering losses are neglected during its generation [3, 6, 11]. However, the nonlinear nanophotonic structures used to generate the light have lossy modes that leak energy into the surrounding environment. Therefore, the generated light in the lossy modes cannot be in a pure state. Throughout the rest of this paper we refer to the lossy modes of a structure as quasimodes, which are eigenstates of the non-Hermitian linear Hamiltonian, with complex frequencies,  $\widetilde{\omega}_m = \omega_m - i\gamma_m$ , that have a real part,  $\omega_m$ , as well as an imaginary part,  $\gamma_m$ , that quantifies the energy leakage.

Theoretical work including the effects of scattering loss has been done on the generation of entangled states and

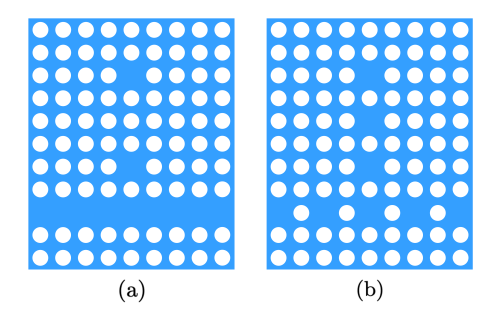


FIG. 1: Schematics of two different square lattice photonic crystal slab structures of interest (the white circles are air-holes). The first structure (a) consists of two coupled cavities side-coupled to a defect-waveguide. The second structure (b) consists of three coupled high-Q cavities, side-coupled to a coupled-resonator optical waveguide.

squeezed states via SFWM or PDC in ring resonators [12–14], nonlinear waveguides [15], and coupled-cavities in a photonic crystal slab [16, 17]. Recently, it was proven that the generated light in the quasimodes in such systems takes the form of a multimode squeezed thermal state (MSTS) [18], where the thermal part of the state captures the photon loss. It was demonstrated that the amount of squeezing in the MSTS is less than it is in a MSVS with the same squeezing parameter, due to an increase in quadrature noise arising from scattering loss during the generation and propagation processes. Although these studies have not focused on generating cluster states, the MSTS solution opens up a path to study cluster states generated by SFWM in lossy structures.

The MSTS solution has thus far only been proven for the case when the quasimodes are orthogonal, which will only occur for the modes in structures that have high symmetry, such as the ring modes of a ring resonator or the Bloch modes of a defect waveguide in a photonic crystal slab. In these structures, the quasimodes are eigenmodes of symmetry operators (e.g. rotational or translational) that make quasimodes of different frequency orthogonal. As a result, their spatial overlap integral is zero. The quasimodes of a general lossy structure are not orthogonal and thus the MSTS solution has only

<sup>\*</sup> colin.vendromin@queensu.ca

been shown to be valid for a restricted set of idealized high-symmetry structures.

There are many structures of interest that have quasimodes that are highly nonorthogonal; two examples are shown in Fig. 1. In Fig. 1(a), pairs of signal and idler photons can be generated in the quasimodes of the two coupled cavities by pumping them from above with a Gaussian beam. The defect coupled-resonator optical waveguide (CROW) couples the generated light out the of cavities, but it also breaks the symmetry of the lattice, causing the modes to be nonorthogonal. The structure in Fig. 1(b) incorporates a CROW for the pump, which resonantly couples to side-coupled nonlinear resonant cavities, where it generates pairs of signal and idler photons. There are three modes in the side-coupled cavities, one for the pump and one each for the generated signal and idler photons. We have calculated the quasimodes for the structure in Fig. 1 (b) and found that the overlap between some of the modes can be as high as 10%. This system is of particular interest as it incorporates the pump, signal, and idler channel as well as the nonlinear resonant structure all in one integrated system. Therefore, it is important to find an efficient and accurate way to model the nonlinear generation in such systems.

In this work, we prove that the density operator for the generated light in a lossy system with a set of quasimodes takes the form of a MSTS, even when the quasimodes are nonorthogonal, but the thermal portion of the density operator is not diagonal in the quasimode basis, but in a new orthogonalized basis. We apply our theory to a simplified version of the structure in Fig. 1(a) to generate a two-mode squeezed thermal state in the two nonorthogonal quasimodes of the resonant structure which have an overlap of about 80%, and demonstrate agreement with numerical approaches as well as the strong effect of the nonorthogonality.

The nonorthogonality of the quasimodes prevent the usual quantization procedure, but there are two approaches to quantizing them. The first approach is based on a Green's function quantization method, and is applicable to general absorptive and lossy media [19]. The second approach is to quantize the electric field in the standard way using the lossless normal modes, and then to project onto the lossy quasimodes by a non-Hermitian projection operator [20]. The second approach is applicable to non-absorptive media with scattering losses through the open boundaries, and is the one that we use throughout the rest of this paper. It is relatively straightforward to show (see Appendix B) that for the case of SFWM or PDC in a non-absorptive medium with scattering loss, both approaches give the exact same form for the Lindblad master equation for the density operator,  $\widehat{\rho}(t)$ , of the generated light:

$$\frac{d\widehat{\rho}}{dt} = \frac{-i}{\hbar} \left[ \widehat{H}, \widehat{\rho} \right] + \sum_{m,l} \chi_{ml}^{(-)} \left( 2\widehat{a}_l \widehat{\rho} \widehat{a}_m^{\dagger} - \widehat{\rho} \widehat{a}_m^{\dagger} \widehat{a}_l - \widehat{a}_m^{\dagger} \widehat{a}_l \widehat{\rho} \right).$$

Therefore the form of  $\hat{\rho}(t)$  is independent of the quan-Here  $\widehat{H}$  is the Hermitian tization approach used. Hamiltonian, which includes the linear Hamiltonian as well as the nonlinear interaction, and  $\hat{a}_m$  and  $\hat{a}_m^{\dagger}$  are bosonic annihilation and creation operators for photons in the symmetrized modes m, with  $[\hat{a}_m, \hat{a}_l^{\dagger}] = \delta_{ml}$ . The symmetrized modes are linear combinations of the nonorthogonal quasimodes, chosen so that the symmetrized modes are orthogonal, but are no longer eigenstates of the non-Hermetian linear Hamiltonian (see Eq. (B9)). We define  $\chi^{(-)} \equiv \frac{i}{2} (\chi - \chi^{\dagger})$ , where  $\chi$  is the quasimode coupling matrix. The off-diagonal coupling terms in  $\chi$  come from the quasimode nonorthogonality, and have been shown to contribute to the spontaneous emission rate of a quantum dot in a cavity [21, 22]. In our approach, the quasimode coupling matrix is related to the quasimode overlap and the quasimode frequencies with  $\chi \equiv O^{1/2} \widetilde{\omega} O^{-1/2}$ , where O is a matrix of the mode overlaps and  $\widetilde{\boldsymbol{\omega}} \equiv \operatorname{diag}(\widetilde{\omega}_1, \ldots)$  is a diagonal matrix of the quasimode frequencies.

The generation of the light in the cavity system can be modelled with Eq. (1). Numerical solutions to Eq. (1) for the density operator can be obtained by expanding the operators in a basis of Fock states and then integrating the resulting set of coupled differential equations [23]. The number of equations is the square of the dimension of the basis. For example, for a state with Mmodes and a maximum photon number of N, the number of possible Fock states is at least (M+N)!/(M!N!)[24], and the number of equations is the square of this. Thus, for multimode states with many photons there can be an impractical number of equations to solve in order to obtain accurate results for the density matrix, unless dimension reduction techniques are used. Alternatively, instead of solving for the time-dependent density operator, one might be able to calculate the time-dependent expectation value of any mode operators, with only the initial state, using a Heisenberg – Langevin approach generalized to nonorthogonal modes. If one knows beforehand that the state is Gaussian at all times, then it is fully determined by its covariance matrix. Calculating the covariance matrix using the Heisenberg - Langevin approach only requires solving on the order of  $M^2$  coupled differential equations. However, as we shall show, our method only requires one to solve the 3M coupled first-order differential equations for the MSTS parameters. We now present the derivation of our analytic solution to the Lindblad master equation.

Analytic solution to the Lindblad master equation.— We consider a general lossy resonant structure that has a set of discrete nonorthogonal quasimodes, and we let the initial state of the system to be the vacuum state. The squeezed light is generated in the quasimodes by a SFWM interaction, where pairs of signal and idler photons are generated by the annihilation of pairs of pump photons. We take the pump to be a classical electric field that is modelled as a coherent state. Our analytic solution requires that the signal and idler modes are ef-

fectively coupled to a single pump mode, such that we can factorize the nonlinear parameter, for the SFWM interaction, into a part that only depends on the pump and a separate part that only depends on the signal and idler modes. One way to achieve this is to require the pump be in a coherent state,  $|\alpha(t)\rangle$ , in a single quasimode, P, with a time-dependent coherent state parameter given by  $\alpha(t) = \alpha_P(t) \exp(-i\omega_P t)$ , where  $\alpha_P(t)$  is slowly-varying complex temporal envelope and  $\omega_P$  is the pump frequency. Alternatively, this can be achieved in a setup where the structure is pumped from above, e.g. with a Gaussian beam in the free-space continuous modes, but the pump beam modes all have essentially the same nonlinear overlap with a given pair of signal and idler modes (see Ref. [17] and Appendix E). Using the undepleted pump approximation, the nonlinear Hamiltonian for the interaction takes the form

$$\widehat{H}_{\rm NL} = \hbar \alpha^2(t) \sum_{m,l} S_{ml} \widehat{a}_m^{\dagger} \widehat{a}_l^{\dagger} + \text{H.c.}, \qquad (2)$$

where the matrix S is the nonlinear parameter for spontaneous four-wave mixing (see Appendix B).

The generated light satisfies the Lindblad master equation (Eq. (1)), where the system Hamiltonian is defined as,  $\hat{H} \equiv \hat{H}_{\rm L} + \hat{H}_{\rm NL}$ , where the linear Hamiltonian is given by

$$\widehat{H}_L = \hbar \sum_{m,l} \chi_{ml}^{(+)} \widehat{a}_m^{\dagger} \widehat{a}_l, \tag{3}$$

with  $\chi^{(+)} \equiv \frac{1}{2} (\chi + \chi^{\dagger})$ . The main result of this work is that the analytic solution to Eq. (1) can be written in the form of an MSTS, defined as

$$\widehat{\rho}(t) = \widehat{S}(t)\widehat{\rho}_{\rm th}(t)\widehat{S}^{\dagger}(t),$$
 (4)

where  $\hat{S}(t)$  is a unitary multimode squeezing operator and  $\hat{\rho}_{\rm th}(t)$  is a density operator describing a multimode thermal state. As we will show, with the right basis choice,  $\hat{S}(t)$  can be expressed as a product of single-mode squeezing operators, and  $\hat{\rho}_{\rm th}(t)$  can be expressed as a product of single-mode thermal density operators, but the basis required for thermal-state factorization is different than that used to factorize the squeezing operator. Expressing them in this way allows us to derive a set of coupled differential equations that the squeezing parameters and thermal photon numbers for the state must obey

in order for  $\widehat{\rho}(t)$  to be the solution. To express  $\widehat{S}(t)$  as a product of single-mode squeezing operators, we perform a symmetric singular value decomposition of the nonlinear parameter in Eq. (2),  $\mathbf{S} = \mathbf{U} \boldsymbol{\lambda} \mathbf{U}^{\mathrm{T}}$ , where  $\mathbf{U} \mathbf{U}^{\dagger} = 1$  and  $\boldsymbol{\lambda} \equiv \mathrm{diag}(\lambda_1, \ldots)$  is a diagonal matrix of the singular values. Putting this into Eq. (2), we obtain

$$\widehat{H}_{\rm NL} = \hbar \alpha^2(t) \sum_{\mu} \lambda_{\mu} \widehat{B}_{\mu}^{\dagger 2} + \text{H.c.}, \qquad (5)$$

where we define the Schmidt mode creation operators as  $\widehat{B}^{\dagger}_{\mu} \equiv \sum_{m} U_{\mu m} \widehat{a}^{\dagger}_{m}$ , with  $[\widehat{B}_{\mu}, \widehat{B}^{\dagger}_{\nu}] = \delta_{\mu\nu}$ . In order to write  $\widehat{\rho}_{\rm th}(t)$  as a product of single-mode thermal density operators, we perform a singular value decomposition of  $\chi^{(+)}$  (see Eq. (3)),  $\chi^{(+)} = M^{(+)} \omega^{\rm s} M^{(+)\dagger}$ , where  $M^{(+)}M^{(+)\dagger} = 1$  and  $\omega^{\rm s} \equiv {\rm diag}(\omega_1^{\rm s}, \ldots)$  is a diagonal matrix of the singular values. Putting this into Eq. (3), we obtain

$$\widehat{H}_{L} = \hbar \sum_{\kappa} \omega_{\kappa}^{s} \widehat{C}_{\kappa}^{\dagger} \widehat{C}_{\kappa}, \tag{6}$$

where we define the thermal mode creation operators as  $\widehat{C}_{\kappa}^{\dagger} \equiv \sum_{m} M_{\kappa m}^{(+)} \widehat{a}_{m}^{\dagger}$ , with  $[\widehat{C}_{\kappa}, \widehat{C}_{\kappa'}^{\dagger}] = \delta_{\kappa \kappa'}$ .

Now in the Schmidt mode basis,  $\hat{S}(t)$  can be written simply as [18]

$$\widehat{S}(t) = \prod_{\mu} \exp\left(\frac{1}{2}r_{\mu}(t)e^{i\phi_{\mu}(t)}\widehat{B}_{\mu}^{\dagger 2} - \text{H.c.}\right), \quad (7)$$

where  $r_{\mu}(t)$  and  $\phi_{\mu}(t)$  are the squeezing amplitude and the squeezing phase of the  $\mu$ th Schmidt mode. In the thermal mode basis,  $\hat{\rho}_{\rm th}(t)$  can be written simply as

$$\widehat{\rho}_{\rm th}(t) = \prod_{\kappa} \frac{1}{1 + n_{\kappa}(t)} \left( \frac{n_{\kappa}(t)}{1 + n_{\kappa}(t)} \right)^{C_{\kappa}^{\dagger} C_{\kappa}}, \quad (8)$$

where  $n_{\kappa}(t) \equiv \text{Tr}\left[\hat{\rho}_{\text{th}}(t)\hat{C}_{\kappa}^{\dagger}\hat{C}_{\kappa}\right]$  is the average thermal photon number of the thermal mode,  $\kappa$ . The average thermal photon number is not related to thermal effects, but rather captures the process of photon loss due to scattering.

It can be shown (see Appendix C) that requiring that Eq. (4) is the solution to the Lindblad master equation leads to the following coupled differential equations for  $r_{\mu}(t)$ ,  $\phi_{\mu}(t)$ , and  $n_{\kappa}(t)$ :

$$\frac{dr_{\mu}}{dt} = \frac{2}{\hbar} \operatorname{Im} \left[ \alpha^{2}(t) \lambda_{\mu} e^{-i\phi_{\mu}} \right] - 2 \sum_{\nu,\sigma} \cosh\left(r_{\nu}\right) \sinh\left(r_{\sigma}\right) \operatorname{Re}\left[\mathcal{N}_{\mu\nu\sigma}\right], \tag{9}$$

$$\frac{d\phi_{\mu}}{dt} = -2\Omega_{\mu\mu} - \frac{4}{\hbar \tanh(2r_{\mu})} \operatorname{Re}\left[\alpha^{2}(t)\lambda_{\mu}e^{-i\phi_{\mu}}\right] - 2\sum_{\nu,\sigma} \frac{\cosh(r_{\nu})\sinh(r_{\sigma})}{\cosh(r_{\mu})\sinh(r_{\mu})} \operatorname{Im}\left[\mathcal{N}_{\mu\nu\sigma}\right],\tag{10}$$

$$\frac{dn_{\kappa}}{dt} = -2n_{\kappa} \sum_{\nu,\sigma} Y_{\kappa\nu} Y_{\kappa\sigma}^* \Gamma_{\sigma\nu} \cosh(r_{\nu}) \cosh(r_{\sigma}) + 2(1+n_{\kappa}) \sum_{\nu,\sigma} Y_{\kappa\nu} Y_{\kappa\sigma}^* \Gamma_{\nu\sigma} \sinh(r_{\nu}) \sinh(r_{\sigma}) e^{i(\phi_{\nu} - \phi_{\sigma})}, \qquad (11)$$

where  $\Omega_{\mu\mu}$  is the  $\mu$ th Schmidt mode frequency, where  $\Omega \equiv Y^{\dagger}\omega^{s}Y$ , with  $Y \equiv M^{(+)\dagger}U$ , and  $\Gamma \equiv V^{\dagger}\gamma^{s}V$ , where  $V \equiv M^{(-)\dagger}U$ . Here  $M^{(-)}$  is obtained from a singular value decomposition of  $\chi^{(-)}$  (found in the Lindblad master equation, Eq. (1)),  $\chi^{(-)} = M^{(-)}\gamma^{s}M^{(-)\dagger}$ , where  $M^{(-)}M^{(-)\dagger} = 1$  and  $\gamma^{s} \equiv \operatorname{diag}(\gamma_{1}^{s},...)$  is a diagonal matrix of the singular values. For convenience we have also defined

$$\mathcal{N}_{\mu\nu\sigma} \equiv \Gamma_{\sigma\nu} e^{i(\phi_{\sigma} - \phi_{\mu})} \sum_{\kappa,\kappa'} Y_{\kappa\sigma} Y_{\kappa'\nu} Y_{\kappa\mu}^* Y_{\kappa'\mu}^* \frac{n_{\kappa} - n_{\kappa'} + 1}{n_{\kappa} + n_{\kappa'} + 1}.$$
 (12)

The coupled equations Eqs. (9) - (11) can be solved numerically for the parameters  $r_{\mu}(t)$ ,  $\phi_{\mu}(t)$ , and  $n_{\kappa}(t)$  using a Runge Kutta method. For M modes, there are only 3M coupled equations that need to be solved. Using these parameters in Eqs. (4), (7), and (8), the density operator of the MSTS is obtained for all times

Quadrature squeezing of the Schmidt modes.— With the MSTS one can derive simple analytic expressions for the expectation value of observables written in terms of the Schmidt mode operators. As an example, we derive an analytic expression for the quadrature squeezing of the Schmidt modes. We define the quadrature operator

$$\widehat{Q}_{\mu} \equiv e^{i(\omega_P t + \beta_{\mu})} \widehat{B}_{\mu} + e^{-i(\omega_P t + \beta_{\mu})} \widehat{B}_{\mu}^{\dagger}, \qquad (13)$$

where  $\beta_{\mu}$  is the initial phase at t=0. The quantum noise in the quadrature is defined as the variance of the quadrature operator,  $\langle \widehat{Q}_{\mu}^2 \rangle \equiv \text{Tr}(\widehat{Q}_{\mu}^2 \widehat{\rho}(t))$ . Using the MSTS in Eq. (4) it can be shown that the quadrature noise is simply given by

$$\langle \hat{Q}_{\mu}^{2} \rangle = (1 + 2\eta_{\mu\mu}) \sin^{2} (\phi_{\mu}/2 + \omega_{P}t + \beta_{\mu}) e^{2r_{\mu}} + (1 + 2\eta_{\mu\mu}) \cos^{2} (\phi_{\mu}/2 + \omega_{P}t + \beta_{\mu}) e^{-2r_{\mu}}, \quad (14)$$

where we define  $\eta_{\mu\nu}(t) \equiv \sum_{\kappa} Y_{\mu\kappa} n_{\kappa}(t) Y_{\nu\kappa}^*$ . It can be shown that for the Schmidt mode frequencies,  $\Omega_{\mu\mu}$ , that are on resonance with twice the pump frequency, the squeezing phase solution is approximately given by,  $\phi_{\mu}(t) \simeq -2\omega_P t - 2\beta_{\mu}$ , and the amplitude of the oscillations in Eq. (14) are greatly diminished. Thus, close to resonance we obtain the approximate expression,  $\langle \widehat{Q}_{\mu}^2 \rangle \simeq (1+2\eta_{\mu\mu})\,\mathrm{e}^{-2r_{\mu}}$ , which only contains the exponential squeezing factor. The quadrature noise is squeezed below the vacuum noise whenever  $\langle \widehat{Q}_{\mu}^2 \rangle < 1$ . Note that the thermal photon numbers increase the quadrature noise by the factor  $(1+2\eta_{\mu\mu})$ , and thus the squeezing level is less than it is in a pure MSVS with the same squeezing parameter.

Two-mode squeezed thermal state generated in two coupled-cavities in a finite photonic crystal slab.— We now apply our theory to study the generation of a twomode squeezed thermal state in two coupled defect cavities, that are embedded asymmetrically in a finite square lattice photonic crystal slab with the period d (see Fig. 2(a)). This structure has been studied in Refs. [20] and [25] in a different context, and we use the same parameters for the photonic crystal slab here (see Appendix E). We have chosen the system to be asymmetric so that (as we shall see) the two confined quasimodes of the system are nonorthogonal. The individual cavity modes and their frequencies are obtained from finite-difference timedomain (FDTD) calculations using Lumerical. The two confined quasimodes are obtained with a tight-binding model [20], where the individual cavity modes form the

The overlap matrix (see Appendix A) for the two quasimodes for the structure in Fig. 2(a) is

$$O = \begin{bmatrix} 1 & 0.76 - i0.44 \\ 0.76 + i0.44 & 1 \end{bmatrix}, \tag{15}$$

which shows that the quasimodes of different frequency are highly nonorthogonal with a large overlap,  $|O_{12}| = |O_{21}| = 0.88$ . The theoretical upper limit of the overlap is 0.90 (see Appendix A). Thus, our calculation shows that the nonorthogonality between the two modes is nearly at its maximum.

To generate the squeezed state in the coupled-cavities, we take the system to be pumped from above with a 0.43mW Gaussian beam polarized in the y direction that is continuous-wave in time, with frequency  $\omega_P d/(2\pi c) = 0.3027$  (its profile is illustrated by the large shaded circle in Fig. 2(a)). We let its full width at half maximum be 5d (solid line circle). The details of the derivation of the nonlinear parameter S using this Gaussian pump pulse are given in the Appendix E.

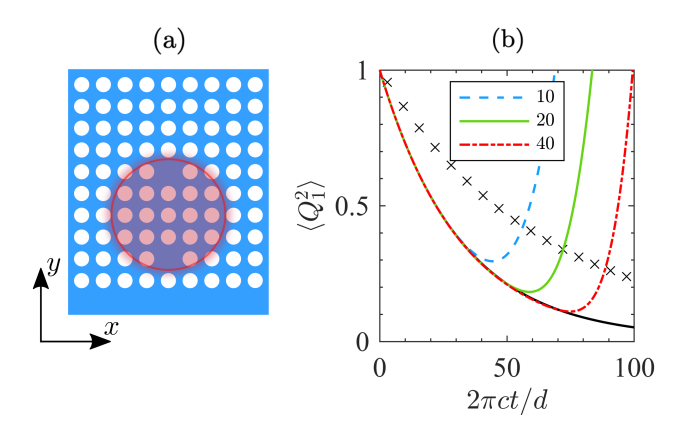


FIG. 2: (a) Schematic of the structure we model to obtain our results. This is a simplified version of Fig. 1 (b). It consists of two coupled-cavities in a finite photonic crystal slab that are embedded asymmetrically in a square lattice. The cavities are pumped from above with a Gaussian pulse. Its transverse profile is shown as the large shaded circle (where the solid line circle is its full width at half maximum). (b) Quadrature noise,  $\langle Q_1^2 \rangle$ , calculated using the two-mode squeezed thermal state (solid black line), and using QuTiP with 10, 20, and 40 Fock basis states in each mode. Also, we plot the quadrature noise when the overlap is excluded  $(O_{12} = O_{21} = 0)$  (crosses).

We solve the coupled-equations Eqs. (9) - (11) using a fourth-order Runge-Kutta method. For t < 0 the state is the vacuum state, and then at t = 0 the continuous-wave pump is turned on and the generation process begins. For the two-mode system, it takes about 0.5 seconds on a standard PC to solve the coupled-equations.

In order to demonstrate the validity and efficiency of our results, we compare them with numerical calculations done using QuTiP [26], which is a software package that can solve the Lindblad master equation numerically (even for nonorthogonal quasimodes) by expanding operators in a Fock basis. In Fig. 2(b) we plot the quadrature noise in the first quasimode,  $\langle Q_1^2 \rangle$ , calculated using Eq. (14) and QuTiP. The quadrature noise is squeezed below the vacuum noise,  $\langle Q_1^2 \rangle < 1$ , for all times. In the plot, the oscillations in the noise shown in Eq. (14) are not evident, because the pump is resonant, such that the squeezing phase is approximately given by  $\phi_1(t) \simeq -2\omega_P t - \pi$ . The Fock basis results converge to the MSTS result when

the number of Fock basis states in each quasimode is increased sufficiently. For our system, we see convergence for  $t < 70d/(2\pi c)$  using 40 Fock states in each mode. With this number of states, the density operator is represented as a  $1600 \times 1600$  matrix in the Fock basis, and thus one needs to solve as many as 2.56 million coupled equations (*i.e.*, one for each element of the density matrix). However, with our approach we only need to solve 6 equations. At  $t = 70d/(2\pi c)$  there are on average 3 photons generated, and at  $t = 100d/(2\pi c)$  there are 9.

Finally, we demonstrate that the non-zero overlap between the quasimodes in Eq. (15) has a significant effect on the quadrature squeezing. We do this by excluding the overlap between the two quasimodes, i.e.  $O_{12} = O_{21} = 0$ , while keeping all other values the same. This quantifies the effect that the overlap has on the results, but it is not intended to represent a physical situation for the structure. In Fig. 2(b) we plot  $\langle Q_1^2 \rangle$  without the overlap (crosses); as can be seen, for  $t = 100d/(2\pi c)$  there is an increase in the noise of 6.3 dB above the correct value.

In this section we have shown that 1) the numerical results using our method agree with those using a Fock basis, as long as enough states are included; 2) when the photon number becomes large, the simulations using a Fock basis take a prohibitively long time to run; and 3) our approach remains accurate and fast even when the effects of the mode nonorthogonality is large.

Conclusion. — We have proven that the analytic solution to the Lindblad master equation for light generated by a nonlinearity in the quasimodes of a general multimode structure is the density operator for an MSTS, even when the mode nonorthogonality is included. Our approach can make it more feasible to study the important problem of nonlinear optical generation of entangled squeezed states in multimode lossy nanocavities, since the number of equations to solve depends only linearly on the total number of system modes. Our analytic solution opens up a path to investigate and optimize the generation and evolution of cluster states made from a general mixed Gaussian state.

#### ACKNOWLEDGEMENTS

This work was supported by Queen's University and the Natural Sciences and Engineering Research Council of Canada (NSERC).

S. Lloyd and S. L. Braunstein, Quantum computation over continuous variables, Phys. Rev. Lett. 82, 1784 (1999).

<sup>[2]</sup> P. van Loock, C. Weedbrook, and M. Gu, Building gaussian cluster states by linear optics, Phys. Rev. A 76, 032321 (2007).

<sup>[3]</sup> J. Zhang and S. L. Braunstein, Continuous-variable gaussian analog of cluster states, Phys. Rev. A 73, 032318

<sup>(2006).</sup> 

<sup>[4]</sup> S. Yokoyama, R. Ukai, S. C. Armstrong, C. Sornphiphatphong, T. Kaji, S. Suzuki, J. Yoshikawa, H. Yonezawa, N. C. Menicucci, and A. Furusawa, Ultra-large-scale continuous-variable cluster states multiplexed in the time domain, Nat. Photonics 7, 982 (2013).

<sup>[5]</sup> M. V. Larsen, X. Guo, C. R. Breum, J. S. Neergaard-Nielsen, and U. L. Andersen, Deterministic generation of

- a two-dimensional cluster state, Science 366, 369 (2019).
- [6] N. C. Menicucci, S. T. Flammia, H. Zaidi, and O. Pfister, Ultracompact generation of continuous-variable cluster states, Phys. Rev. A 76, 010302 (2007).
- [7] B. H. Wu, R. N. Alexander, S. Liu, and Z. Zhang, Quantum computing with multidimensional continuousvariable cluster states in a scalable photonic platform, Phys. Rev. Res. 2, 023138 (2020).
- [8] N. C. Menicucci, S. T. Flammia, and O. Pfister, One-way quantum computing in the optical frequency comb, Phys. Rev. Lett. 101, 130501 (2008).
- [9] J. Roslund, R. Medeiros de Araújo, S. Jiang, C. Fabre, and N. Treps, Wavelength-multiplexed quantum networks with ultrafast frequency combs, Nat. Photonics 8, 109 (2014).
- [10] C. Reimer, S. Sciara, P. Roztocki, M. Islam, L. R. Cortés, Y. Zhang, B. Fischer, S. Loranger, R. Kashyap, A. Cino, S. T. Chu, B. E. Little, D. J. Moss, L. Caspani, W. J. Munro, J. Azaña, M. Kues, and R. Morandotti, Highdimensional one-way quantum processing implemented on d-level cluster states, Nat. Phys. 15, 148 (2019).
- [11] N. C. Menicucci, S. T. Flammia, and P. van Loock, Graphical calculus for gaussian pure states, Phys. Rev. A 83, 042335 (2011).
- [12] Z. Vernon and J. E. Sipe, Spontaneous four-wave mixing in lossy microring resonators, Phys. Rev. A 91, 053802 (2015).
- [13] C. Vendromin and M. M. Dignam, Optimization of a lossy microring resonator system for the generation of quadrature-squeezed states, Phys. Rev. A 102, 023705 (2020).
- [14] C. Vendromin and M. M. Dignam, Continuous-variable entanglement in a two-mode lossy cavity: An analytic solution, Phys. Rev. A 103, 022418 (2021).
- [15] L. G. Helt, M. J. Steel, and J. E. Sipe, Spontaneous parametric downconversion in waveguides: What's loss got to do with it?, New J. Phys. 17, 013055 (2014).
- [16] M. K. Dezfouli and M. M. Dignam, Photon-pair generation in lossy coupled-resonator optical waveguides via spontaneous four-wave mixing, Phys. Rev. A 95, 033815 (2017).
- [17] H. Seifoory, L. G. Helt, J. E. Sipe, and M. M. Dignam, Counterpropagating continuous-variable entangled states in lossy coupled-cavity optical waveguides, Phys. Rev. A 100, 033839 (2019).
- [18] C. Vendromin and M. M. Dignam, Simple way to incorporate loss when modeling multimode-entangled-state generation, Phys. Rev. A 105, 063707 (2022).
- [19] S. Franke, S. Hughes, M. Kamandar Dezfouli, P. T. Kristensen, K. Busch, A. Knorr, and M. Richter, Quantization of quasinormal modes for open cavities and plasmonic cavity quantum electrodynamics, Phys. Rev. Lett. 122, 213901 (2019).
- [20] D. P. Fussell and M. M. Dignam, Quasimode-projection approach to quantum-dot-photon interactions in photonic-crystal-slab coupled-cavity systems, Phys. Rev. A 77, 053805 (2008).
- [21] M. M. Dignam, D. P. Fussell, M. J. Steel, C. Martijn de Sterke, and R. C. McPhedran, Spontaneous emission suppression via quantum path interference in coupled microcavities, Phys. Rev. Lett. 96, 103902 (2006).
- [22] J. Ren, S. Franke, and S. Hughes, Connecting classical and quantum mode theories for coupled lossy cavity resonators using quasinormal modes, ACS Photonics 9, 138

- (2022).
- [23] D. Manzano, A short introduction to the lindblad master equation, AIP Advances 10, 025106 (2020).
- [24] M. Gregg and M. Richter, Efficient and exact numerical approach for many multi-level systems in open system CQED, New J. Phys. 18, 043037 (2016).
- [25] M. M. Dignam and M. K. Dezfouli, Photon-quantum-dot dynamics in coupled-cavity photonic crystal slabs, Phys. Rev. A 85, 013809 (2012).
- [26] J. R. Johansson, P. D. Nation, and F. Nori, Qutip: An open-source python framework for the dynamics of open quantum systems, Comp. Phys. Comm. 183, 1760 (2012).
- [27] N. K. Hon, R. Soref, and B. Jalali, The third-order non-linear optical coefficients of si, ge, and  $\mathrm{Si}_{1-x}\mathrm{Ge}_x$  in the midwave and longwave infrared, J. Appl. Phys. **110**, 011301 (2011).

#### Appendix A: Nonorthogonal quasimodes

In this section, we define the lossy nonorthogonal quasimodes of a resonant structure and their spatial overlap. We also derive an expression for the upper bound on the overlap.

We consider an open dielectric system with out-going boundary conditions. The positive frequency part of the electric field in a lossy quasimode m takes the form [20]

$$\boldsymbol{E}^{(+)}(\boldsymbol{r},t) = \boldsymbol{N}_m(\boldsymbol{r}) e^{-i\widetilde{\omega}_m t}, \tag{A1}$$

where  $N_m(r)$  is the spatial profile of the quasimode, and ts complex frequency is  $\widetilde{\omega}_m \equiv \omega_m - i\gamma_m$ . Each quasimode is a solution to the Helmholtz equation:

$$\nabla \times \nabla \times \boldsymbol{N}_{m}(\boldsymbol{r}) - \frac{\widetilde{\omega}_{m}^{2}}{c^{2}} \epsilon(\boldsymbol{r}) \boldsymbol{N}_{m}(\boldsymbol{r}) = 0, \quad (A2)$$

where  $\epsilon(\mathbf{r})$  is the real, relative dielectric function for the structure. We define the inner product between two quasimodes of different frequency  $\widetilde{\omega}_m$  and  $\widetilde{\omega}_l$  as

$$\langle \mathbf{N}_m | \mathbf{N}_l \rangle \equiv \int d^3 \mathbf{r} \epsilon(\mathbf{r}) \mathbf{N}_m^*(\mathbf{r}) \cdot \mathbf{N}_l(\mathbf{r}).$$
 (A3)

The quasimodes are calculated within a computational volume that is bounded by perfectly-matched layers (PMLs) in order to simulate open boundary conditions. The integral in Eq. (A3) is done over the computational volume only. Throughout this work, the fields in the PMLs are excluded from all integrals.

The normalized quasimode overlap is

$$O_{ml} \equiv \frac{\langle \mathbf{N}_m | \mathbf{N}_l \rangle}{\sqrt{\langle \mathbf{N}_m | \mathbf{N}_m \rangle \langle \mathbf{N}_l | \mathbf{N}_l \rangle}}.$$
 (A4)

Note that  $\boldsymbol{O}$  is a Hermitian matrix. For a general system of coupled-cavities, the off-diagonal elements of the overlap are non-zero. Therefore, the quasimodes form a nonorthogonal basis.

As we shall show below, the upper bound on the overlap in Eq. (A4) is derived by requiring that the quasimodes satisfy outgoing-wave boundary conditions at infinity. We will show it is given by

$$\left|O_{ml}\right|^2 \le \frac{4\gamma_m \gamma_l}{(\omega_m - \omega_l)^2 + (\gamma_m + \gamma_l)^2}.$$
 (A5)

Using this result one can get some idea if the overlap between two quasimodes is negligible or not. For example, if the difference between the real parts of the frequencies is much larger than the sum of the imaginary parts (i.e.  $|\omega_m - \omega_l| \gg \gamma_m + \gamma_l$ ), then the overlap is approximately given by  $|O_{ml}|^2 \approx 4\gamma_m \gamma_l/(\omega_m - \omega_l)^2$ , and this will approach zero the larger the frequency difference is. Therefore, quasimodes that are separated in frequency but much more than their line-widths will have a negligible overlap and will be approximately orthogonal. Alternatively, if two quasimodes are close in frequency (i.e.  $\omega_m \approx \omega_l$ ), then the overlap is approximately given by  $|O_{ml}|^2 \approx 4\gamma_m \gamma_l/(\gamma_m + \gamma_l)^2$ , which will be close to one. Therefore, quasimodes that are close in frequency can generally have a large overlap, unless some symmetry forbids it. We find that this overlap can be very large in systems of coupled-cavities in a photonic crystal slab, such as the two-defect structure discussed in the paper.

Now we derive Eq. (A5). First, we combine Eqs. (A2) and (A3) to obtain

$$\frac{1}{c^2} \left( \widetilde{\omega}_m^{*2} - \widetilde{\omega}_l^2 \right) \langle \mathbf{N}_m | \mathbf{N}_l \rangle = \mathcal{A}_{ml} - \mathcal{A}_{lm}^*, \tag{A6}$$

where

$$\mathcal{A}_{ml} \equiv \int d^3 \boldsymbol{r} \left[ \nabla \times \nabla \times \boldsymbol{N}_m^*(\boldsymbol{r}) \right] \cdot \boldsymbol{N}_l(\boldsymbol{r}). \tag{A7}$$

Immediately, we see that if  $\mathcal{A}$  is a Hermitian matrix, then  $O_{ml}$  must be zero and the quasimodes are orthogonal. However, we show that  $\mathcal{A}$  is not Hermitian due to the lossy nature of the quasimodes. Using the vector calculus identity  $\nabla \cdot (\mathbf{P} \times \mathbf{Q}) = (\nabla \times \mathbf{P}) \cdot \mathbf{Q} - (\nabla \times \mathbf{Q}) \cdot \mathbf{P}$ , with  $\mathbf{P} \equiv \nabla \times \mathbf{N}_m^*$  and  $\mathbf{Q} \equiv \mathbf{N}_l$ , Eq. (A7) can be written as

$$\mathcal{A}_{ml} = \int d^3 \boldsymbol{r} \left[ \nabla \times \boldsymbol{N}_l(\boldsymbol{r}) \right] \cdot \left[ \nabla \times \boldsymbol{N}_m^*(\boldsymbol{r}) \right]$$

$$+ \int_{\partial V} \left[ (\nabla \times \boldsymbol{N}_m^*(\boldsymbol{r})) \times \boldsymbol{N}_l(\boldsymbol{r}) \right] \cdot d\boldsymbol{A}, \qquad (A8)$$

where we have used the divergence theorem on the last term in Eq. (A8), with  $\partial V$  defined as the surface boundary of the computational volume V and dA is an infinitesimal area element on and normal to the surface boundary. The first term in Eq. (A8) is clearly Hermitian, however the surface integral in the second term is not. It is this integral of the quasimodes on the surface boundary that causes the problem to be non Hermitian and the quasimodes to be nonorthogonal. Using Eq. (A8), the

right-hand side of Eq. (A7) can be written as

$$\mathcal{A}_{ml} - \mathcal{A}_{lm}^* = \int_{\partial V} \left[ (\nabla \times \boldsymbol{N}_m^*(\boldsymbol{r})) \times \boldsymbol{N}_l(\boldsymbol{r}) - (\nabla \times \boldsymbol{N}_l(\boldsymbol{r})) \times \boldsymbol{N}_m^*(\boldsymbol{r}) \right] \cdot d\boldsymbol{A}.$$
(A9)

The surface boundary is taken to be the edge of the computational volume (but excluding the PMLs), and it must be far from any sources, such that the modes are given by out-going waves. In the standard treatment of electric and magnetic field normal modes, the surface integrals in Eq. (A9) are zero because the normal modes decay to zero at infinity. This is the origin of the orthogonality of the normal modes. However, due to the lossy nature of the quasimodes, mathematically they do not decay to zero at the surface boundary. This is because at the surface the quasimodes are out-going waves, with a complex wavevector that causes them to diverge. Therefore, the surface integral in Eq. (A6) quantifies the nonorthogonality of the quasimodes.

To evaluate Eq. (A9) we take the surface boundary to be a sphere of radius r, and we let  $r \to \infty$ . We assume that at infinity there is a homogeneous background dielectric material of a constant index of refraction. We let the quasimodes be given by spherical outgoing waves as  $r \to \infty$ , that are polarized tangentially to the surface of the sphere. They have the form

$$\mathbf{N}_{m}(r,\theta,\phi) = \left[h_{m\theta}(\theta,\phi)\hat{\epsilon}_{\theta} + h_{m\phi}(\theta,\phi)\hat{\epsilon}_{\phi}\right] \frac{\mathrm{e}^{i\tilde{k}_{m}r}}{r}, \text{ (A10)}$$

where  $\widetilde{k}_m = (\omega_m - i\gamma_m)n/c$  is the complex wavevector, where n is the index of refraction of the homogeneous background dielectric. The components of the quasimodes in the  $\hat{\epsilon}_{\theta}$  and  $\hat{\epsilon}_{\phi}$  directions are  $h_{m\theta}(\theta,\phi)$  and  $h_{m\phi}(\theta,\phi)$ , respectively, and they do not depend on r. There is no component of the quasimodes in the  $\hat{\epsilon}_r$  direction. Note that the combination of  $i\tilde{k}$  in Eq. (A10) causes the quasimodes to exponentially increase as  $r \to \infty$ . This is because the exponential increases faster than 1/r decreases. Putting Eq. (A10) into Eq. (A9), defining  $d\mathbf{A} \equiv r^2 \sin(\theta) d\theta d\phi \hat{\epsilon}_r$ , and doing the cross-products in spherical coordinates, we obtain

$$\mathcal{A}_{ml} - \mathcal{A}_{lm}^* = \frac{i}{n^2} \langle \boldsymbol{h}_m | \boldsymbol{h}_l \rangle \left( \widetilde{k}_m^* + \widetilde{k}_l \right) e^{-i(\widetilde{k}_m^* - \widetilde{k}_l)r}, \tag{A11}$$

where  $\langle \boldsymbol{h}_m | \boldsymbol{h}_l \rangle$  is the inner product on the surface boundary, defined by

$$\langle \boldsymbol{h}_m | \boldsymbol{h}_l \rangle \equiv n^2 \iint \boldsymbol{h}_m^*(\theta, \phi) \cdot \boldsymbol{h}_l(\theta, \phi) \sin(\theta) d\theta d\phi.$$
 (A12)

Putting Eq. (A11) into Eq. (A6), the quasimode inner product can be written as

$$\langle \mathbf{N}_m | \mathbf{N}_l \rangle = i \langle \mathbf{h}_m | \mathbf{h}_l \rangle \frac{e^{-i(\widetilde{k}_m^* - \widetilde{k}_l)r}}{\widetilde{k}_m^* - \widetilde{k}_l},$$
 (A13)

where we used the fact that  $\widetilde{\omega}_m^{*2} - \widetilde{\omega}_l^2 = (c/n)^2 (\widetilde{k}_m^* + \widetilde{k}_l)(\widetilde{k}_m^* - \widetilde{k}_l)$ . Therefore if the inner product on the boundary is zero, then the quasimodes are orthogonal. Putting Eq. (A13) into Eq. (A4), it can be shown that the absolute value squared of the overlap is given by

$$|O_{ml}|^2 = \frac{\left|\left\langle \mathbf{h}_m | \mathbf{h}_l \right\rangle\right|^2}{\left\langle \mathbf{h}_m | \mathbf{h}_m \right\rangle \left\langle \mathbf{h}_l | \mathbf{h}_l \right\rangle} \frac{4\gamma_m \gamma_l}{(\omega_m - \omega_l)^2 + (\gamma_m + \gamma_l)^2}.$$
(A14)

Now using the Cauchy-Schwarz inequality,  $|\langle \boldsymbol{h}_m | \boldsymbol{h}_l \rangle|^2 \le \langle \boldsymbol{h}_m | \boldsymbol{h}_m \rangle \langle \boldsymbol{h}_l | \boldsymbol{h}_l \rangle$ , the upper bound of the overlap in Eq. (A14) is

$$|O_{ml}|^2 = \frac{4\gamma_m \gamma_l}{(\omega_m - \omega_l)^2 + (\gamma_m + \gamma_l)^2}.$$
 (A15)

Therefore,  $\left|O_{ml}\right|^2$  is always less than this upper bound, and we obtain the inequality in Eq. (A5).

#### Appendix B: The Lindblad master equation

In this section, we present the Lindblad master equation, that was derived using the quasimode projection technique [20], written in terms of the quasimode operators. We show that we obtain the exact same form for the Lindblad master equation that was derived using a different quantization approach using quasi-normal modes [19].

The system Hamiltonian can be written as

$$\widehat{H} = \widehat{H}_{L} + \widehat{H}_{NL}. \tag{B1}$$

In the basis of the discrete quasimodes, it can be shown that the linear part is given by [20]

$$\widehat{H}_{L} = \hbar \sum_{m,l} \widetilde{\omega}_{l} O_{ml} \widehat{c}_{m}^{\dagger} \widehat{c}_{l}, \qquad (B2)$$

where  $\hat{c}_m^{\dagger}$  and  $\hat{c}_m$  are the creation and annihilation operators for photons in the *m*th quasimode. They satisfy the commutation relation

$$\left[\hat{c}_m, \hat{c}_l^{\dagger}\right] = O_{ml}^{-1},\tag{B3}$$

where  $\mathbf{O}^{-1}$  is the inverse of the overlap matrix of Eq. (A4), satisfying

$$1 = \mathbf{O}^{-1}\mathbf{O}. \tag{B4}$$

We let the nonlinear Hamiltonian account for the spontaneous four-wave mixing (SFWM) interaction that generates the squeezed light. We take the pump to be a classical field in a single quasimode, P. Using the undepleted pump approximation, the nonlinear Hamiltonian is given by

$$\widehat{H}_{\rm NL} = \hbar \alpha^2(t) \sum_{m,l} G_{ml} \widehat{c}_m^{\dagger} \widehat{c}_l^{\dagger} + \text{H.c.}, \qquad (B5)$$

where  $\alpha(t) = |\alpha_P| e^{-i\omega_P t}$  is the pump amplitude with frequency  $\omega_P$ , and  $G_{ml}$  is the nonlinear parameter for SFWM, given by

$$G_{ml} \equiv \frac{9\hbar\omega_P}{16\epsilon_0} \sum_{i,j,k,h} \sqrt{\widetilde{\omega}_m^* \widetilde{\omega}_l^*} \times \int d^3 \boldsymbol{r} \chi_{ijkh}^{(3)}(\boldsymbol{r}) N_{mi}^*(\boldsymbol{r}) N_{lj}^*(\boldsymbol{r}) N_{Pk}(\boldsymbol{r}) N_{Ph}(\boldsymbol{r}),$$
(B6)

where i, j, k, and h are the Cartesian components of the spatially-dependent third-order nonlinear susceptibility tensor  $\chi^{(3)}_{ijkh}(\mathbf{r})$ .

The Lindblad master equation for the density operator  $\hat{\rho}(t)$  was derived in previous work, using the quasimode projection approach, for nonorthogonal quasimodes. It is given by [25]

$$\frac{d\widehat{\rho}}{dt} = \frac{-i}{\hbar} \left[ \widehat{H}_{L}^{(+)} + \widehat{H}_{NL}, \widehat{\rho} \right] 
+ \frac{i}{2} \sum_{m,l} \left( \widetilde{\omega}_{l} - \widetilde{\omega}_{m}^{*} \right) O_{ml} \left( 2\widehat{c}_{l} \widehat{\rho} \widehat{c}_{m}^{\dagger} - \widehat{\rho} \widehat{c}_{m}^{\dagger} \widehat{c}_{l} - \widehat{c}_{m}^{\dagger} \widehat{c}_{l} \widehat{\rho} \right),$$
(B7)

where  ${\cal H}_L^{(+)}$  is the Hermitian part of the linear Hamiltonian and is defined as

$$H_L^{(+)} \equiv \frac{\hbar}{2} \sum_{m,l} (\widetilde{\omega}_l + \widetilde{\omega}_m^*) O_{ml} \widehat{c}_m^{\dagger} \widehat{c}_l.$$
 (B8)

The expressions for the quantized Hamiltonian and the Lindblad master equation are written in terms of the quasimode annihilation and creation operators, which do not obey the standard commutation relation for bosons. This is a result of the quantization approach used. In a different quantization approach that uses quasi-normal modes [19], the Hamiltonian and Lindblad master equation are written in terms of photon operators that do obey the standard commutator. Now we show that we can connect the two approaches by doing a symmetrization transformation of the quasimode operators (similar to Ref. [19])

$$\widehat{a}_m \equiv \sum_{l} O_{ml}^{1/2} \widehat{c}_l, \tag{B9}$$

such that these operators have the standard commutation relation

$$[\widehat{a}_m, \widehat{a}_l^{\dagger}] = \delta_{ml},$$
 (B10)

which can be derived using Eqs. (B3) and (B4). Writing  $H_L^{(+)}$  in Eq. (B8) in terms of these operators, we obtain

$$H_L^{(+)} = \hbar \sum_{m,l} \chi_{ml}^{(+)} \hat{a}_m^{\dagger} \hat{a}_l,$$
 (B11)

and for the Lindblad master equation in Eq. (B7), we obtain

$$\frac{d\widehat{\rho}}{dt} = \frac{-i}{\hbar} \left[ \widehat{H}_{L}^{(+)} + \widehat{H}_{NL}, \widehat{\rho} \right] 
+ \sum_{m,l} \chi_{ml}^{(-)} \left( 2\widehat{a}_{l} \widehat{\rho} \widehat{a}_{m}^{\dagger} - \widehat{\rho} \widehat{a}_{m}^{\dagger} \widehat{a}_{l} - \widehat{a}_{m}^{\dagger} \widehat{a}_{l} \widehat{\rho} \right).$$
(B12)

Here  $\chi^{(-)}$  and  $\chi^{(+)}$  are Hermitian matrices defined as

$$\chi^{(-)} \equiv \frac{i}{2} \left( \chi - \chi^{\dagger} \right),$$
(B13)

$$\chi^{(+)} \equiv \frac{1}{2} \left( \chi + \chi^{\dagger} \right),$$
(B14)

where,

$$\chi \equiv O^{1/2} \widetilde{\omega} O^{-1/2}, \tag{B15}$$

where  $\widetilde{\boldsymbol{\omega}} \equiv \operatorname{diag}(\widetilde{\omega}_1,\ldots)$ . The matrices  $\chi_{ml}^{(+)}$  and  $\chi_{ml}^{(-)}$  give the coupling between different quasimodes in the Hamiltonian and Lindblad dissipator. The coupling will be strong for quasimodes that have a large overlap. Note that if the quasimodes are orthogonal to each other, with  $\boldsymbol{O}=1$ , then  $\boldsymbol{\chi}^{(-)}=\operatorname{diag}(\gamma_1,\ldots)$  and  $\boldsymbol{\chi}^{(+)}=\operatorname{diag}(\omega_1,\ldots)$  are just proportional to the imaginary and real parts of the complex frequency  $\widetilde{\omega}_m$ . This will give the usual form of the Hamiltonian and Lindblad dissipator for orthogonal modes.

The nonlinear Hamiltonian in Eq. (B5) can be written using  $\hat{a}_m$  and  $\hat{a}_m^{\dagger}$  as

$$\widehat{H}_{\rm NL} = \hbar \alpha^2(t) \sum_{m,l} S_{ml} \widehat{a}_m^{\dagger} \widehat{a}_l^{\dagger} + \text{H.c.},$$
 (B16)

where S is the nonlinear parameter defined by

$$S \equiv O^{-1/2}G \left[O^{-1/2}\right]^{\mathrm{T}}.$$
 (B17)

Note that S is also a complex symmetric matrix, with  $S^{T} = S$ .

Equations (3) and (B12), that were derived using the quasimode projection approach, have the exact same form as those that were derived using a different quantization approach using the quasi-normal mode formalism (see Eqs. (28a) and (30) in Ref.[22]). Therefore, the form of the density operator solution to the Lindblad master equation does not depend on the quasimode quantization approach used, and so our analytic solution is applicable to both approaches.

## 1. The diagonalized form of the Lindblad master equation

In this subsection we write the Lindblad master equation in Eq. (B12) in its diagonal form. It is important to do this, because it will help us derive the analytic solution to the Lindblad master equation in the next section.

The diagonalization can be achieved by decomposing the quasimode coupling matrix  $\chi^{(-)}$  with the singular value decomposition

$$\boldsymbol{\chi}^{(-)} = \boldsymbol{M}^{(-)} \boldsymbol{\gamma}^{\mathrm{s}} \boldsymbol{M}^{(-)\dagger}, \tag{B18}$$

where  $M^{(-)}M^{(-)\dagger} = 1$  and  $\gamma^{\rm s} \equiv {\rm diag}(\gamma_1^{\rm s},...)$  is a diagonal matrix of the singular values. Putting Eq. (B18) into Eq. (B12), we obtain

$$\frac{d\widehat{\rho}}{dt} = \frac{-i}{\hbar} \left[ \widehat{H}_{L}^{(+)} + \widehat{H}_{NL}, \widehat{\rho} \right] 
+ \sum_{\sigma} \gamma_{\sigma}^{s} \left( 2\widehat{A}_{\sigma}\widehat{\rho}\widehat{A}_{\sigma}^{\dagger} - \widehat{\rho}\widehat{A}_{\sigma}^{\dagger}\widehat{A}_{\sigma} - \widehat{A}_{\sigma}^{\dagger}\widehat{A}_{\sigma}\widehat{\rho} \right), \quad (B19)$$

which is the diagonal form of the Lindblad master equation. We define the creation operator

$$\widehat{A}_{\sigma}^{\dagger} \equiv \sum_{m} M_{m\sigma}^{(-)} \widehat{a}_{m}^{\dagger}, \tag{B20}$$

that statisfies the commutator  $[\widehat{A}_{\sigma}, \widehat{A}_{\sigma'}^{\dagger}] = \delta_{\sigma\sigma'}$ .

# Appendix C: Analytic solution to the Lindblad master equation

In this section, we show that the analytic solution to the Lindblad master equation for SFWM is the density operator,  $\hat{\rho}(t)$ , for a multimode squeezed thermal state, given in Eq. (4). To prove that this is the solution, we require that  $\hat{\rho}(t)$  to be a solution of

$$1 = \widehat{\rho}_{\rm th}^{-1/2}(t)\widehat{S}^{\dagger}(t)\widehat{\rho}(t)\widehat{S}(t)\widehat{\rho}_{\rm th}^{-1/2}(t), \tag{C1}$$

where we used the fact that  $\hat{S}^{\dagger}(t)\hat{S}(t) = 1$ . Since Eq. (C1) is true for all times, if we take the time derivative of both sides, we obtain

$$0 = \widehat{\rho}_{\rm th}^{1/2} \widehat{S}^{\dagger} \frac{d\widehat{S}}{dt} \widehat{\rho}_{\rm th}^{-1/2} - \widehat{\rho}_{\rm th}^{-1/2} \widehat{S}^{\dagger} \frac{d\widehat{S}}{dt} \widehat{\rho}_{\rm th}^{1/2}$$
$$+ 2 \frac{d\widehat{\rho}_{\rm th}^{-1/2}}{dt} \widehat{\rho}_{\rm th}^{1/2} + \widehat{\rho}_{\rm th}^{-1/2} \widehat{S}^{\dagger} \frac{d\widehat{\rho}}{dt} \widehat{S} \widehat{\rho}_{\rm th}^{-1/2}, \qquad (C2)$$

where we dropped the time-dependence of the operators for convenience. We obtain the coupled-equations Eqs. (9) - (11) by simplifying the four terms on the right-hand side of Eq. (C2). Our strategy is to put the expressions for  $\widehat{S}(t)$ ,  $\widehat{\rho}_{\rm th}(t)$ , and  $d\widehat{\rho}(t)/dt$  into Eq. (C2). As we will show, the right-hand side can be written in terms of three Schrödinger operators:  $\widehat{A}_{\sigma}^{\dagger}\widehat{A}_{\nu}$ ,  $\widehat{Q}_{\sigma\nu}$  (Eq. (C12)), and  $\widehat{\mathcal{P}}_{\sigma\nu}$  (Eq. (C13)), that are common to each term, and are multiplied by time-dependent coefficients that depend on  $r_{\mu}(t)$ ,  $\phi_{\mu}(t)$ , and  $n_{\mu}(t)$  and their first time-derivatives. To satisfy Eq. (C2), and obtain the coupled-equations, we let the coefficients in front of the three operators equal zero.

We define the following terms that help in the derivation:

$$T_1 \equiv 2 \frac{d\widehat{\rho}_{\rm th}^{-1/2}}{dt} \widehat{\rho}_{\rm th}^{1/2},\tag{C3}$$

$$T_2 \equiv \widehat{\rho}_{\rm th}^{1/2} \widehat{S}^{\dagger} \frac{d\widehat{S}}{dt} \widehat{\rho}_{\rm th}^{-1/2} - \widehat{\rho}_{\rm th}^{-1/2} \widehat{S}^{\dagger} \frac{d\widehat{S}}{dt} \widehat{\rho}_{\rm th}^{1/2}, \tag{C4}$$

$$T_3 \equiv \widehat{\rho}_{\rm th}^{-1/2} \widehat{S}^{\dagger} \frac{d\widehat{\rho}}{dt} \widehat{S} \widehat{\rho}_{\rm th}^{-1/2}. \tag{C5}$$

Using the definition of  $\widehat{\rho}_{th}(t)$  in Eq. (8), it can be shown that  $T_1$  simplifies to

$$T_{1} = -\sum_{\kappa} \frac{1}{n_{\kappa}(1+n_{\kappa})} \frac{dn_{\kappa}}{dt} \sum_{\sigma,\nu} W_{\kappa\sigma}^{*} W_{\kappa\nu} \widehat{A}_{\sigma}^{\dagger} \widehat{A}_{\nu}$$
$$+ \sum_{\kappa} \frac{1}{1+n_{\kappa}} \frac{dn_{\kappa}}{dt}. \tag{C6}$$

Moving on to  $T_2$ , we first simplify the time-derivative of

the squeezing operator. It can be shown that [18]

$$\widehat{S}^{\dagger} \frac{d\widehat{S}}{dt} = \sum_{\mu} \left( \frac{i}{2} \sinh^{2}(r_{\mu}) \frac{d\phi_{\mu}}{dt} \left( 2\widehat{B}_{\mu}^{\dagger} \widehat{B}_{\mu} + 1 \right) + \left( \frac{1}{2} \frac{dr_{\mu}}{dt} + \frac{i}{4} \sinh(2r_{\mu}) \frac{d\phi_{\mu}}{dt} \right) e^{i\phi_{\mu}} \widehat{B}_{\mu}^{\dagger 2} - \left( \frac{1}{2} \frac{dr_{\mu}}{dt} - \frac{i}{4} \sinh(2r_{\mu}) \frac{d\phi_{\mu}}{dt} \right) e^{-i\phi_{\mu}} \widehat{B}_{\mu}^{2} \right). \quad (C7)$$

Now to simplify  $T_2$  we need to perform the thermal transformations on Eq. (C7). These can be done with

$$\widehat{\rho}_{\rm th}^{\pm 1/2} \widehat{B}_{\mu} \widehat{\rho}_{\rm th}^{\mp 1/2} = \sum_{\kappa, \sigma} Y_{\kappa\mu}^* x_{\kappa}^{\mp 1/2} W_{\kappa\sigma} \widehat{A}_{\sigma}, \qquad (C8)$$

$$\widehat{\rho}_{\rm th}^{\pm 1/2} \widehat{B}_{\mu}^{\dagger} \widehat{\rho}_{\rm th}^{\mp 1/2} = \sum_{\kappa,\sigma} Y_{\kappa\mu} x_{\kappa}^{\pm 1/2} W_{\kappa\sigma}^* \widehat{A}_{\sigma}^{\dagger}, \qquad (C9)$$

where  $oldsymbol{W} \equiv oldsymbol{Y} oldsymbol{V}^\dagger$  and we define

$$x_{\mu} \equiv \frac{n_{\mu}}{1 + n_{\mu}}.\tag{C10}$$

Using Eqs. (C8) and (C7), it can be shown that  $T_2$  simplifies to

$$T_{2} = \sum_{\sigma,\nu} \left( F_{\sigma\nu} \widehat{A}_{\sigma}^{\dagger} \widehat{A}_{\nu} + \text{Re}[D_{\sigma\nu}] \widehat{\mathcal{Q}}_{\sigma\nu} + \text{Im}[D_{\sigma\nu}] \widehat{\mathcal{P}}_{\sigma\nu} \right),$$
(C11)

where we define two Schrödinger operators

$$\widehat{\mathcal{Q}}_{\sigma\nu} \equiv \widehat{A}_{\sigma} \widehat{A}_{\nu} + \widehat{A}_{\sigma}^{\dagger} \widehat{A}_{\nu}^{\dagger}, \tag{C12}$$

$$\widehat{\mathcal{P}}_{\sigma\nu} \equiv -i\widehat{A}_{\sigma}\widehat{A}_{\nu} + i\widehat{A}_{\sigma}^{\dagger}\widehat{A}_{\nu}^{\dagger}, \tag{C13}$$

and the time-dependent coefficients

$$F_{\sigma\nu} \equiv \sum_{\mu,\kappa,\kappa'} i \sinh^2(r_{\mu}) \frac{d\phi_{\mu}}{dt} Y_{\kappa\mu} Y_{\kappa'\mu}^* W_{\kappa\sigma} W_{\kappa'\nu}^* \left[ x_{\kappa}^{1/2} x_{\kappa'}^{-1/2} - x_{\kappa}^{-1/2} x_{\kappa'}^{1/2} \right], \tag{C14}$$

$$D_{\sigma\nu} \equiv \sum_{\mu,\kappa,\kappa'} \left( \frac{1}{2} \frac{dr_{\mu}}{dt} + \frac{i}{4} \sinh(2r_{\mu}) \frac{d\phi_{\mu}}{dt} \right) e^{i\phi_{\mu}} Y_{\kappa\mu} Y_{\kappa'\mu} W_{\kappa\sigma}^* W_{\kappa'\nu}^* \left[ x_{\kappa}^{1/2} x_{\kappa'}^{1/2} - x_{\kappa}^{-1/2} x_{\kappa'}^{-1/2} \right], \tag{C15}$$

where  $\text{Re}[D_{\sigma\nu}]$  and  $\text{Im}[D_{\sigma\nu}]$  are the real and imaginary parts of  $D_{\sigma\nu}$ .

Moving on to  $T_3$ , the squeezing transformation of the Lindblad master equation in Eq. (B19) can be done using

$$\widehat{S}^{\dagger}\widehat{A}_{\sigma}\widehat{S} = \sum_{\mu} V_{\sigma\mu} \widehat{S}^{\dagger}\widehat{B}_{\mu}\widehat{S}, \tag{C16}$$

$$\widehat{S}^{\dagger}\widehat{C}_{\kappa}\widehat{S} = \sum_{\mu} Y_{\kappa\mu} \widehat{S}^{\dagger}\widehat{B}_{\mu}\widehat{S},\tag{C17}$$

where the squeezing transformation of the  $\widehat{B}_{\mu}$  operators is

$$\widehat{S}^{\dagger}\widehat{B}_{\mu}\widehat{S} = \cosh(r_{\mu})\widehat{B}_{\mu} + e^{i\phi_{\mu}}\sinh(r_{\mu})\widehat{B}_{\mu}^{\dagger}. \tag{C18}$$

After performing the squeezing transformation in  $T_3$ , the remaining thermal transformation can be done using Eq. (C8). Doing this we obtain

$$T_{3} = \sum_{\sigma,\nu} \left( K_{\sigma\nu} \widehat{A}_{\sigma}^{\dagger} \widehat{A}_{\nu} + \operatorname{Re}[E_{\sigma\nu}] \widehat{\mathcal{Q}}_{\sigma\nu} + \operatorname{Im}[E_{\sigma\nu}] \widehat{\mathcal{P}}_{\sigma\nu} \right) + 2 \sum_{\nu,\sigma,\nu'} \Gamma_{\sigma\nu} \cosh(r_{\sigma}) \cosh(r_{\nu}) Y_{\sigma\nu'}^{*} Y_{\nu\nu'} x_{\nu'} - 2 \sum_{\nu} \Gamma_{\nu\nu} \sinh^{2}(r_{\nu}), \tag{C19}$$

where

$$E_{\sigma\nu} = \sum_{\mu,\mu',\kappa',\kappa} e^{i\phi_{\mu'}} \cosh(r_{\mu}) \sinh(r_{\mu'}) Y_{\kappa'\mu} Y_{\kappa\mu'} W_{\kappa'\sigma}^* W_{\kappa\nu}^*$$

$$\times \left( i\Omega_{\mu\mu'} \left[ x_{\kappa'}^{1/2} x_{\kappa}^{1/2} - x_{\kappa'}^{-1/2} x_{\kappa}^{-1/2} \right] - \Gamma_{\mu'\mu} \left[ x_{\kappa'}^{1/2} x_{\kappa}^{1/2} + x_{\kappa'}^{-1/2} x_{\kappa}^{-1/2} - 2x_{\kappa}^{-1/2} x_{\kappa'}^{1/2} \right] \right)$$

$$+ i \sum_{\mu,\kappa',\kappa} \left( \alpha^2(t) \lambda_{\mu} \cosh^2(r_{\mu}) + \alpha^{*2}(t) \lambda_{\mu}^* \sinh^2(r_{\mu}) e^{2i\phi_{\mu}} \right) Y_{\kappa'\mu} Y_{\kappa\mu} W_{\kappa'\sigma}^* W_{\kappa\nu}^* \left[ x_{\kappa'}^{1/2} x_{\kappa}^{1/2} - x_{\kappa'}^{-1/2} x_{\kappa}^{-1/2} \right]$$

$$K_{\sigma\nu} = \sum_{\mu,\mu',\kappa',\kappa} Y_{\kappa'\mu} Y_{\kappa\mu'}^* W_{\kappa'\sigma}^* W_{\kappa\nu} \cosh(r_{\mu'}) \cosh(r_{\mu})$$

$$\times \left( i\Omega_{\mu\mu'} \left[ x_{\kappa'}^{1/2} x_{\kappa}^{-1/2} - x_{\kappa'}^{-1/2} x_{\kappa}^{1/2} \right] - \Gamma_{\mu'\mu} \left[ x_{\kappa'}^{1/2} x_{\kappa}^{-1/2} + x_{\kappa'}^{-1/2} x_{\kappa}^{1/2} - 2x_{\kappa'}^{1/2} x_{\kappa}^{1/2} \right] \right)$$

$$+ \sum_{\mu,\mu',\kappa',\kappa} Y_{\kappa'\mu} Y_{\kappa\mu'}^* W_{\kappa'\sigma}^* W_{\kappa\nu} \sinh(r_{\mu'}) \sinh(r_{\mu}) e^{i(\phi_{\mu} - \phi_{\mu'})}$$

$$\times \left( i\Omega_{\mu'\mu} \left[ x_{\kappa'}^{1/2} x_{\kappa}^{-1/2} - x_{\kappa'}^{-1/2} x_{\kappa}^{1/2} \right] - \Gamma_{\mu\mu'} \left[ x_{\kappa'}^{1/2} x_{\kappa}^{-1/2} + x_{\kappa'}^{-1/2} x_{\kappa}^{1/2} - 2x_{\kappa'}^{-1/2} x_{\kappa}^{-1/2} \right] \right)$$

$$- 2i \sum_{\mu,\kappa',\kappa} \cosh(r_{\mu}) \sinh(r_{\mu}) \left( \alpha^2(t) \lambda_{\mu} e^{i\phi_{\mu}} + \alpha^{*2}(t) \lambda_{\mu}^* e^{-i\phi_{\mu}} \right) Y_{\kappa'\mu} Y_{\kappa\mu}^* W_{\kappa'\sigma}^* W_{\kappa\nu} \left[ x_{\kappa'}^{-1/2} x_{\kappa}^{-1/2} - x_{\kappa'}^{1/2} x_{\kappa}^{-1/2} \right]$$
(C22)

Now in order for Eq. (C2) to be satisfied, the three terms must add to zero,  $T_1 + T_2 + T_3 = 0$ . We achieve this by making the time-dependent coefficients in front of each operator  $\widehat{A}_{\sigma}^{\dagger}\widehat{A}_{\nu}$ ,  $\widehat{Q}_{\sigma_{\nu}}$ , and  $\widehat{P}_{\sigma_{\nu}}$  equal zero. First, we let the sum of the coefficients in front of  $\widehat{Q}_{\sigma\nu}$  and  $\widehat{P}_{\sigma\nu}$  in  $T_2$  and  $T_3$  equal zero

$$0 = \operatorname{Re}[D_{\sigma\nu}] + \operatorname{Re}[E_{\sigma\nu}],\tag{C23}$$

$$0 = \operatorname{Im}[D_{\sigma\nu}] + \operatorname{Im}[E_{\sigma\nu}]. \tag{C24}$$

These are satisfied if we let

$$D_{\sigma\nu} = -E_{\sigma\nu}.\tag{C25}$$

As we shall see, solving Eq. (C25) gives the differential equations for  $dr_{\mu}/dt$  and  $d\phi_{\mu}/dt$ . To start, we multiply both sides of Eq. (C25) by  $\sum_{\sigma,\nu} W_{\kappa\sigma}W_{\kappa'\nu}$  and use Eq.(C15) to obtain

$$\left[x_{\kappa}^{1/2}x_{\kappa'}^{1/2} - x_{\kappa}^{-1/2}x_{\kappa'}^{-1/2}\right] \sum_{\mu} \left(\frac{1}{2}\frac{dr_{\mu}}{dt} + \frac{i}{4}\sinh(2r_{\mu})\frac{d\phi_{\mu}}{dt}\right) e^{i\phi_{\mu}}Y_{\kappa\mu}Y_{\kappa'\mu} = -\sum_{\sigma,\nu} W_{\kappa\sigma}W_{\kappa'\nu}E_{\sigma\nu},\tag{C26}$$

where we used the fact that  $\mathbf{W}^{\dagger}\mathbf{W} = 1$ . Multiplying Eq. (C26) by  $\sum_{\kappa,\kappa'} Y_{\kappa\mu'}^* Y_{\kappa'\mu'}^*$  and using the orthogonality relation  $\mathbf{Y}^{\dagger}\mathbf{Y} = 1$ , we obtain

$$\frac{1}{2}\frac{dr_{\mu}}{dt} + \frac{i}{4}\sinh(2r_{\mu})\frac{d\phi_{\mu}}{dt} = -e^{-i\phi_{\mu}}\sum_{\kappa,\kappa'}\frac{Y_{\kappa\mu}^{*}Y_{\kappa'\mu}^{*}}{x_{\kappa}^{1/2}x_{\kappa'}^{1/2} - x_{\kappa}^{-1/2}x_{\kappa'}^{-1/2}}\sum_{\sigma,\nu}W_{\kappa\sigma}W_{\kappa'\nu}E_{\sigma\nu}.$$
 (C27)

Equating the real and imaginary parts of both sides of Eq. (C27) gives the following equations for  $dr_{\mu}/dt$  and  $d\phi_{\mu}/dt$ :

$$\frac{dr_{\mu}}{dt} = -\sum_{\kappa,\kappa',\sigma,\nu} \frac{e^{-i\phi_{\mu}} Y_{\kappa\mu}^* Y_{\kappa'\mu}^* W_{\kappa\sigma} W_{\kappa'\nu} E_{\sigma\nu} + e^{i\phi_{\mu}} Y_{\kappa\mu} Y_{\kappa'\mu} W_{\kappa\sigma}^* W_{\kappa'\nu}^* E_{\sigma\nu}^*}{x_{\kappa'}^{1/2} x_{\kappa'}^{1/2} - x_{\kappa}^{-1/2} x_{\kappa'}^{-1/2}},$$
(C28)

$$\frac{d\phi_{\mu}}{dt} = \frac{2i}{\sinh(2r_{\mu})} \sum_{\kappa,\kappa',\sigma,\nu} \frac{e^{-i\phi_{\mu}} Y_{\kappa\mu}^* Y_{\kappa'\mu}^* W_{\kappa\sigma} W_{\kappa'\nu} E_{\sigma\nu} - e^{i\phi_{\mu}} Y_{\kappa\mu} Y_{\kappa'\mu} W_{\kappa\sigma}^* W_{\kappa'\nu}^* E_{\sigma\nu}^*}{x_{\kappa'}^{1/2} x_{\kappa'}^{1/2} - x_{\kappa}^{-1/2} x_{\kappa'}^{-1/2}}.$$
 (C29)

Now to simplify Eqs. (C28) and (C29) we focus on the first term in the sum. Using the expression for  $E_{\sigma\nu}$  in Eq. (C20), we obtain

$$\sum_{\kappa,\kappa',\sigma,\nu} \frac{e^{-i\phi\mu} Y_{\kappa\mu}^* Y_{\kappa'\mu}^* W_{\kappa\sigma} W_{\kappa'\nu} E_{\sigma\nu}}{x_{\kappa'}^{1/2} x_{\kappa'}^{1/2} - x_{\kappa'}^{-1/2} x_{\kappa'}^{-1/2}} = \sum_{\kappa,\kappa',\mu',\sigma'} e^{i(\phi_{\sigma'} - \phi_{\mu})} \cosh(r_{\mu'}) \sinh(r_{\sigma'}) Y_{\kappa\sigma'} Y_{\kappa'\mu'} Y_{\kappa\mu}^* Y_{\kappa'\mu}^* \\
\times \left( i\Omega_{\mu'\sigma'} - \Gamma_{\sigma'\mu'} \frac{x_{\kappa'}^{-1/2} x_{\kappa}^{-1/2} + x_{\kappa'}^{1/2} x_{\kappa}^{1/2} - 2x_{\kappa}^{-1/2} x_{\kappa'}^{1/2}}{x_{\kappa'}^{1/2} x_{\kappa'}^{1/2} - x_{\kappa}^{-1/2} x_{\kappa'}^{-1/2}} \right) \\
+ i e^{-i\phi_{\mu}} \sum_{\kappa,\kappa',\mu'} \left( \alpha^{2}(t) \lambda_{\mu'} \cosh^{2}(r_{\mu'}) + \alpha^{*2}(t) \lambda_{\mu'}^* \sinh^{2}(r_{\mu'}) e^{2i\phi_{\mu'}} \right) Y_{\kappa\mu'} Y_{\kappa'\mu'} Y_{\kappa\mu}^* Y_{\kappa'\mu}^* Y_$$

Using Eq. (C10) we can write Eq. (C30) in terms of the thermal photon numbers as

$$\sum_{\kappa,\kappa',\sigma,\nu} \frac{e^{-i\phi_{\mu}} Y_{\kappa\mu}^{*} Y_{\kappa\mu}^{*} W_{\sigma\kappa}^{*} W_{\nu\kappa'}^{*} E_{\sigma\nu}}{x_{\kappa'}^{1/2} x_{\kappa'}^{1/2} - x_{\kappa}^{-1/2} x_{\kappa'}^{-1/2}} = i \left(\alpha^{2}(t) \lambda_{\mu} \cosh^{2}(r_{\mu}) e^{-i\phi_{\mu}} + \alpha^{*2}(t) \lambda_{\mu}^{*} \sinh^{2}(r_{\mu}) e^{i\phi_{\mu}}\right) + i \Omega_{\mu\mu} \cosh(r_{\mu}) \sinh(r_{\mu})$$

$$+ \sum_{\kappa,\kappa',\mu',\sigma'} e^{i(\phi_{\sigma'} - \phi_{\mu})} \cosh(r_{\mu'}) \sinh(r_{\sigma'}) Y_{\kappa\sigma'} Y_{\kappa'\mu'} Y_{\kappa\mu}^{*} Y_{\kappa'\mu}^{*} \Gamma_{\sigma'\mu'} \frac{n_{\kappa} - n_{\kappa'} + 1}{n_{\kappa'} + n_{\kappa} + 1}$$
(C31)

The complex conjugate of Eq. (C31) is

$$\sum_{\kappa,\kappa',\sigma,\nu} \frac{e^{i\phi_{\mu}} Y_{\kappa\mu} Y_{\kappa'\mu} W_{\sigma\kappa} W_{\nu\kappa'} E_{\sigma\nu}^*}{x_{\kappa'}^{1/2} x_{\kappa'}^{1/2} - x_{\kappa}^{-1/2} x_{\kappa'}^{-1/2}} = -i \left( \alpha^2(t) \lambda_{\mu} \sinh^2(r_{\mu}) e^{-i\phi_{\mu}} + \alpha^{*2}(t) \lambda_{\mu}^* \cosh^2(r_{\mu}) e^{i\phi_{\mu}} \right) - i \Omega_{\mu\mu} \cosh(r_{\mu}) \sinh(r_{\mu}) 
+ \sum_{\kappa,\kappa',\mu',\sigma'} e^{-i(\phi_{\sigma'} - \phi_{\mu})} \cosh(r_{\mu'}) \sinh(r_{\sigma'}) Y_{\kappa\sigma'}^* Y_{\kappa'\mu'}^* Y_{\kappa\mu} Y_{\kappa'\mu} \Gamma_{\sigma'\mu'} \frac{n_{\kappa} - n_{\kappa'} + 1}{n_{\kappa'} + n_{\kappa} + 1},$$
(C32)

where we used the fact that  $\Omega_{\mu\mu}^* = \Omega_{\mu\mu}$ . Putting Eqs. (C31) and (C32) into Eqs. (C28) and (C29) give the equations for  $dr_{\mu}/dt$  and  $d\phi_{\mu}/dt$  in the text, Eqs. (9) and (10).

Now we derive the equation for  $dn_{\mu}/dt$ . To do this, we let the sum of the coefficients in front of the operators  $\widehat{A}_{\sigma}^{\dagger}\widehat{A}_{\nu}$  in  $T_1$ ,  $T_2$ , and  $T_3$  be zero. Doing this, we obtain the equation

$$0 = -\sum_{\kappa} \frac{1}{n_{\kappa}(1 + n_{\kappa})} \frac{dn_{\kappa}}{dt} W_{\kappa\sigma}^* W_{\kappa\nu} + F_{\sigma\nu} + K_{\sigma\nu}.$$
 (C33)

Multiplying Eq. (C33) by  $\sum_{\sigma\nu} W_{\kappa'\sigma} W_{\kappa'\nu}^*$  and using

 $\mathbf{W}^{\dagger}\mathbf{W} = 1$ , we obtain

$$\frac{1}{n_{\kappa}(1+n_{\kappa})}\frac{dn_{\kappa}}{dt} = \sum_{\sigma\nu} W_{\kappa\sigma}W_{\kappa\nu}^* F_{\sigma\nu} + \sum_{\sigma\nu} W_{\kappa\sigma}W_{\kappa\nu}^* K_{\sigma\nu}.$$
(C34)

The first term on the right-hand side of Eq. (C34) is zero, which can be proved by using Eq. (C14) and  $\mathbf{W}^{\dagger}\mathbf{W}=1$ . For the second term, it can be shown that by putting Eq. (C21) into Eq. (C34) we obtain

$$\frac{1}{1+n_{\kappa}}\frac{dn_{\kappa}}{dt} = -\frac{2n_{\kappa}}{1+n_{\kappa}}\sum_{\nu,\sigma}Y_{\kappa\nu}Y_{\kappa\sigma}^{*}\Gamma_{\sigma\nu}\cosh(r_{\nu})\cosh(r_{\sigma}) + 2\sum_{\nu,\sigma}Y_{\kappa\nu}Y_{\kappa\sigma}^{*}\Gamma_{\nu\sigma}\sinh(r_{\nu})\sinh(r_{\sigma})e^{i(\phi_{\nu}-\phi_{\sigma})}, \quad (C35)$$

which is Eq. (11) in the main text.

Finally we have to show that the sum of the coefficients in front of the identity operator in  $T_1$  and  $T_3$  is zero. Collecting the appropriate coefficients from  $T_1$  and  $T_3$ , we obtain

$$0 = \sum_{\kappa} \frac{1}{1 + n_{\kappa}} \frac{dn_{\kappa}}{dt} + 2 \sum_{\nu, \sigma, \kappa} \Gamma_{\sigma\nu} \cosh(r_{\sigma}) \cosh(r_{\nu}) Y_{\kappa\sigma}^* Y_{\kappa\nu} \frac{n_{\kappa}}{1 + n_{\kappa}} - 2 \sum_{\nu} \Gamma_{\nu\nu} \sinh^2(r_{\nu}). \tag{C36}$$

Putting Eq. (C35) into Eq. (C36) and using the fact that  $Y^{\dagger}Y = 1$ , it can be shown that Eq. (C36) is satisfied.

Therefore we have proven that the multimode squeezed thermal state is the solution to the Lindblad master equation, and we derived three coupled-equations for the squeezing amplitude, squeezing phase, and thermal photon numbers.

## Appendix D: Solving the coupled equations from an initial vacuum state

In this section, we discuss how to solve the coupled-equations (see Eqs. (9) - (11) in the main text) for a system that initially starts in the *vacuum state*. At time t = 0 the vacuum state is defined by

$$r_{\mu}(0) = 0,\tag{D1}$$

$$n_{\kappa}(0) = 0, \tag{D2}$$

for all  $\mu$  and  $\kappa$ . Putting these initial conditions into Eq. (9), we obtain

$$\dot{r}_{\mu}(0) = \frac{2 |\alpha(0)|^2 |\lambda_{\mu}|}{\hbar} \sin(-\phi_{\mu}(0) + \theta_{\mu}),$$
 (D3)

where we define

$$\alpha(t) = \alpha_P(t) \exp(-i\omega_P t),$$
 (D4)

and

$$\lambda_{\mu} = |\lambda_{\mu}| \exp(i\theta_{\mu}), \tag{D5}$$

where  $\theta_{\mu}$  is a real number. We choose the initial squeezing phase,  $\phi_{\mu}(0)$ , to be

$$\phi_{\mu}(0) = \theta_{\mu} - \frac{\pi}{2},\tag{D6}$$

such that is maximizes the squeezing amplitude at the next time-step,  $r_{\mu}(\Delta t)$ :

$$r_{\mu}(\Delta t) = \frac{2 |\alpha(0)|^2 |\lambda_{\mu}|}{\hbar} \Delta t + O\left((\Delta t)^2\right). \tag{D7}$$

Now, let us move on to the equation for the squeezing phase, Eq. (10). It is easily shown that using Eqs. (D1), (D2), and (D6) will result in the second and third terms in Eq. (10) being indeterminate (0/0). Thus, at t=0, we write this equation as

$$\dot{\phi}_{\mu}(0) = -2\Omega_{\mu\mu} - \zeta_{\mu},\tag{D8}$$

where we let  $\zeta_{\mu}$  be the indeterminate form. We are unable to solve these equations unless we define  $\zeta_{\mu}$ . We define  $\zeta_{\mu}$  by requiring that the derivatives of the squeezing phase at  $t = \Delta t$  and t = 0 are the same,

$$\dot{\phi}_{\mu}(\Delta t) = \dot{\phi}_{\mu}(0),\tag{D9}$$

such that initially the squeezing phase is a linear function of time. Putting Eqs. (D1), (D2), (D6), and (D7) into Eq. (10) and using the fact that  $n_{\kappa}(\Delta t) = 0$  (which can be proven by writing Eq. (11) as a difference equation and using the initial conditions) it can be shown that

$$\dot{\phi}_{\mu}(\Delta t) = -2\omega_P + \zeta_{\mu}. \tag{D10}$$

Using Eq. (D10) in Eq. (D9), the indeterminate form  $\zeta_{\mu}$  is defined as

$$\zeta_{\mu} = -\Omega_{\mu\mu} + \omega_P. \tag{D11}$$

To solve the coupled-equations Eqs. (9) - (11) we use Matlab's ode45 function, that is based on a Runge-Kutta method. The initial conditions that we use for the squeezing amplitudes, thermal photon numbers, and squeezing phases are in Eqs. (D1), (D2), and (D6). We have to write an additional condition in the code that imposes the condition that at t=0 the derivatives of the squeezing phases are equal to  $\dot{\phi}_{\mu}(0)=-\Omega_{\mu\mu}-\omega_{P}$ , otherwise the program will return a division-by-zero error (as discussed above). The solution is sensitive to the initial squeezing phases  $\phi_{\mu}(0)$ . It is crucial that they are set to precisely the values given in Eq. (D6). However, we find that the initial value of the derivative of the phase  $\dot{\phi}_{\mu}(0)$  has little impact on the final solution, since it quickly settles to the correct value, given by  $-\Omega_{\mu\mu}-\omega_{P}$ .

#### Appendix E: Details for the two-cavity system results

In this section, we give the details on how we obtain our results for the two-cavity system in the paper. Specifically, we give the physical dimensions of the photonic crystal slab and its material properties, and we derive the nonlinear parameter for SFWM using a Gaussian pump.

We start by giving the details of the structure in Fig. 2(a). The structure is placed in a computational volume of  $13d \times 14d \times 3d$ , where d=480nm is the lattice period. The dielectric slab is parallel to the xy plane and centered at z=0. It is made from silicon with an index of n=1

3.4 and has a thickness of 0.6d. The photonic crystal is created by periodically drilling airholes (shown as white circles) of radius 0.35d into the silicon slab. The photonic crystal is finite in the x-y plane, with 10 periods in the x-y direction and 9 periods in the y-direction. The individual cavities are formed by removing an airhole.

We apply perfectly-matched layers (PMLs) to the boundary of the computational volume to simulate the transmission of energy into a continuum of modes. For the top (T) and bottom (B) individual cavity modes, we obtain the frequencies  $\widetilde{\Omega}_T d/(2\pi c) = 0.3027 - i5.62 \times 10^{-5} \, (Q_T = 2691)$  and  $\widetilde{\Omega}_B d/(2\pi c) = 0.3028 - i9.54 \times 10^{-4} \, (Q_B = 159)$ . Note that  $Q_B$  is less than  $Q_T$ , since the bottom cavity mode leaks into the dielectric slab more. The quasimode frequencies that are obtained from tight-binding [20], where the individual cavity modes form the basis, are  $\widetilde{\omega}_1 d/(2\pi c) = 0.3026 - i3.12 \times 10^{-4} \, (Q_1 = 485)$  and  $\widetilde{\omega}_2 d/(2\pi c) = 0.3029 - i6.93 \times 10^{-4} \, (Q_2 = 218)$ .

Following the presentation of H. Seifoory et. al. in Ref. [17] we now give the details on the Gaussian pump that is used to generate the squeezed light in the quasimodes. As was mentioned in the letter, the system is pumped from above with a Gaussian beam polarized in the y direction. The beam is focused between the two cavities at z=0 and has a Gaussian transverse profile given by

$$f(x,y) \equiv \frac{1}{\sqrt{\pi W_0}} \exp\left[-\frac{2\pi^2}{W_0^2} \left((x-x_0)^2 + y^2\right)\right],$$
 (E1)

where  $W_0$  is the spot size at z = 0 and  $x_0$  is the position on the x axis where the pulse is at its maximum. The full width at half maximum (FWHM) is related to the spot size with FWHM =  $\sqrt{\ln(2)}W_0/\pi$ .

Next we derive the nonlinear parameter for SFWM for the Gaussian beam. We assume the slab thickness is much smaller than the curvature of the optical wavefront, such that it does not have a significant effect on the pump. We can thus take the pump modes to be plane waves in free space, polarized in the y direction

$$N_{qy}(\mathbf{r}) = e^{i\mathbf{q}\cdot\mathbf{r}},\tag{E2}$$

where  $\boldsymbol{q}$  is a continuous index that labels the different modes in three dimensions. We make the undepleted pump approximation, and let the pump quasimode annihilation operators,  $\hat{c}_{\boldsymbol{q}}$ , be replaced by their expectation value using the coherent state amplitude for the Gaussian beam

$$\langle \alpha(t) | \hat{c}_{\mathbf{q}} | \alpha(t) \rangle \equiv |\alpha_P| \alpha(q_x, q_y) \beta(q_z) \exp\left(-i\omega_{|\mathbf{q}|}t\right),$$
(E3)

where the frequency  $\omega_{|q|}$  is real since the pump is in free-space modes and  $|q|^2 \equiv q_x^2 + q_y^2 + q_z^2$ . The function

$$\alpha(q_x, q_y) = \iint dx dy f(x, y) e^{-i(q_x x + q_y y)}, \quad (E4)$$

is the Fourier transform of the transverse profile f(x, y), given in Eq. (E1). It is normalized according to  $\iint dq_x dq_y |\alpha(q_x, q_y)|^2 = 1.$  The function  $\beta(q_z)$  is sharply peaked at the value  $q_P$ 

$$\beta(q_z) \equiv \sqrt{\frac{L}{\sqrt{\pi}}} \exp\left(-\frac{L^2}{2}(q_z - q_P)^2\right),$$
 (E5)

where  $L \equiv 3d$  is the height of the computational volume. It is chosen, such that

$$\int dq_z |\beta(q_z)|^2 = 1.$$
 (E6)

The average photon number for the pump is

$$N_P \equiv \int d^3 \boldsymbol{q} \langle \alpha(t) | \, \hat{c}_{\boldsymbol{q}}^{\dagger} \hat{c}_{\boldsymbol{q}} | \alpha(t) \rangle$$
 (E7)

$$= |\alpha_P|^2, \tag{E8}$$

which follows from the normalization of  $\alpha(q_x, q_y)$  and  $\beta(q_z)$ .

In order to write  $\widehat{H}_{\rm NL}$  in the form in Eq. (B5) where the nonlinear parameter,  $G_{ml}$  is independent of time, we assume that near the surface of the slab the pump is propagating dominantly in the z direction, by letting  $|\mathbf{q}| \simeq q_z$ . Thus we replace the frequency  $\omega_{|\mathbf{q}|}$  in Eq. (E3) with  $\omega_{q_z}$ . Then  $\widehat{H}_{\rm NL}$  (Eq. (B5)) can be written

$$\widehat{H}_{\rm NL} = \hbar |\alpha_P|^2 \sum_{m,l} \widehat{c}_m^{\dagger} \widehat{c}_l^{\dagger} \iint d^3 \mathbf{q} d^3 \mathbf{q}' G_{mlqq'} \alpha(q_x, q_y) \beta(q_z) \alpha(q_x', q_y') \beta(q_z') \exp\left(-i[\omega_{q_z} + \omega_{q_z'}]t\right) + \text{H.c.}, \tag{E9}$$

where

$$G_{mlqq'} = \frac{9\hbar}{16\epsilon_0} \sum_{i,j} \sqrt{\widetilde{\omega}_m^* \widetilde{\omega}_l^* \omega_{q_z} \omega_{q_z'}} \int d^3 \boldsymbol{r} \chi_{ijyy}^{(3)}(\boldsymbol{r}) N_{mi}^*(\boldsymbol{r}) N_{lj}^*(\boldsymbol{r}) e^{i(\boldsymbol{q} + \boldsymbol{q}') \cdot \boldsymbol{r}}.$$
 (E10)

We assume that the interaction is strongest within the

slab, and the interaction strength does not vary signifi-

cantly within the slab, such that we can set z = 0 in Eq. (E10), to obtain  $\exp(iq_z z) = 1$ .

The integral in Eq. (E9) can be factored into an integral over  $q_z$  only and a separate integral over  $q_x$  and  $q_y$  only. Doing the integral over  $q_z$  we obtain an overall function of time,  $\alpha(t)$ , for the coherent state, defined as

$$\alpha(t) \equiv |\alpha_P| \sqrt{\frac{L}{2\sqrt{\pi}\omega_P}} \int dq_z \sqrt{\omega_{q_z}} \beta(q_z) \exp(-i\omega_{q_z} t),$$
(E11)

where  $\omega_P \equiv \omega_{q_P}$ . Since  $\beta(q_z)$  is sharply peaked at  $q_P$ , the integral in Eq. (E11) is dominated by a narrow band of  $q_z$  centered on  $q_P$ . Thus we can pull out from the integral the fast oscillating exponential term,  $\exp(-i\omega_P t)$ , and what is left is a slowly-varying function of time. Taking the limit as the height of the computational volume goes to infinity,  $L \to \infty$ , the function  $\alpha(t)$  approaches a continuous-wave, with  $\alpha(t) \simeq |\alpha_P| \exp(-i\omega_P t)$ . Doing the integrals over  $q_x$  and  $q_y$  in Eq. (E9), we obtain the

approximate expression

$$G_{ml} \simeq \frac{9\hbar\omega_P}{16\epsilon_0 V_{\text{eff}}} \sqrt{\widetilde{\omega}_m^* \widetilde{\omega}_l^*} \times \int d^3 \boldsymbol{r} \chi_{yyyy}^{(3)}(\boldsymbol{r}) N_{my}^*(\boldsymbol{r}) N_{ly}^*(\boldsymbol{r}) \left[ f(x,y) \right]^2, \quad (E12)$$

where we define the effective volume  $V_{\rm eff} \equiv \pi W_0^2 L/(2\sqrt{\pi}(2\pi)^4)$ . To obtain this result we assume that only the diagonal components,  $\chi_{yyyy}^{(3)}(\mathbf{r})$ , of the third-order nonlinear tensor for silicon are non-zero [27]. The quasimode profiles  $N_{my}(\mathbf{r})$  and  $N_{ly}(\mathbf{r})$  are obtained from the tight-binding model used in Ref. [20]. Therefore, considering Eqs. (E11) and (E10), we have shown that Eq. (E9) is equivalent to Eq. (B5), as we require.

To obtain our results, we let

$$\frac{9\hbar\omega_P \chi_{yyyy}^{(3)}}{16\epsilon_0 V_{\text{eff}}} |\alpha_P|^2 = 1, \tag{E13}$$

where  $\chi_{yyyy}^{(3)} = 2.45 \times 10^{-19} \mathrm{m}^2 \mathrm{V}^{-2}$  is the third-order nonlinear susceptibility for silicon [27]. Eq. (E13) is satisfied for a spot size of  $W_0 = 20d$ , and an average number of photons in the pump of  $|\alpha_P|^2 = 3.87 \times 10^7$ . We choose this combination of parameters because it produces significant squeezing of the vacuum noise without generating too many photons. Using the nonlinear parameter in Eq. (E12), we can construct the  $\boldsymbol{S}$  matrix in Eq. (B17), and then perform the Takagi factorization on it to get the matrix  $\boldsymbol{U}$  and the singular values  $\boldsymbol{\lambda}$ .